An efficient way to evidence and to measure the metal ions fraction in high power impulse magnetron sputtering (HiPIMS) post- discharge with Pt, Au, Pd and mixed targets

Stéphane Cuynet, Thomas Lecas, Amael Caillard, Pascal Brault

An efficient way to evidence and to measure the metal ions fraction in high power impulse magnetron sputtering (HiPIMS) post-discharge with Pt, Au, Pd and mixed targets

S Cuynet[1]*, T Lecas[1], A Caillard[1] and P Brault[1]

[1] Groupe de Recherche sur l'Energétique des Milieux Ionisés (GREMI), UMR7344 Université d'Orléans – CNRS, 14 rue d'Issoudun BP6744, F-45067 Orléans Cedex 2, France

* CORRESPONDING AUTHOR : stephane.cuynet@univ-orleans.fr, +33 (0)2 3849 4026

KEYWORDS. QCM, HiPIMS, platinum, gold, palladium, argon, krypton, xenon.

Abstract.

The proportion of metal ions in a High Power Impulse Magnetron Sputtering discharge is a key information for the potential development of new materials and new layer architectures deposited by this technique. This paper aims to measure this proportion by using a homemade system consisting of a quartz crystal microbalance and a grid energy analyzer assembly. Such a system yields relevant results on the composition of the post-discharge depending on the nature of the gas (Ar, Kr, Xe) and the target materials (Pt, Pd, Au, $Pt_{50}Au_{50}$ and Pt_5Pd_{95}). In our conditions, the highest proportions of metal ions in the post-discharge are obtained by using Ar gas and reaches 10 %, 12 %, 50 %, 19 % and 88 % for respective Pt, Au, Pd, $Pt_{50}Au_{50}$ and Pt_5Pd_{95} target.

Introduction

High power impulse magnetron sputtering process (HiPIMS) has permitted to accomplish in 15 years some relevant technical advances on materials, especially on structural properties (Kouznetsov 1999; Hovsepian 2014; Ait Aissa 2014; Lin 2014) and on deposit functionalities (Velicu 2012; Ratova 2014; Partridge 2013; Cuynet 2014; Baghriche 2012) on their supports.

This process is relatively easy to implement on conventional magnetron sputtering systems (direct current magnetron sputtering - DCMS) by only replacing the existent power supply by a HIPIMS generator. Only the electrical connections must be properly sized, since HiPIMS current could reach several kA even if the mean power involved during HiPIMS and DCMS discharges are in the same range of values (Anders 2011).

The strength of the HIPIMS process is mainly due to its ability to partially ionize a portion of the vapor phase of the sputtered material (Alami 2005; Samuelsson 2010; Anders 2008). A part of this ionized metal vapor can then be used to modify the properties of the deposited material by applying a potential (negative in the case of positive ions) to the substrate (Cuynet 2014; Konstantinidis 2006; Wang 2015; Nakao 2013). The electrical parameters of the HIPIMS discharge, the environment in which the discharge takes place, the nature of the sputtering target, the plasma gas and the voltage bias applied to the substrate holder are the main operating parameters that will define the final properties of the deposited material. The understanding of the magnetron sputtering method implies in turn to develop ex- and in-situ diagnostic methods which will be able to measure and to collect data on physical phenomena involved in the process. In the HiPIMS process, the nature of the charged species in the deposition chamber, their energies and their proportions are the main quantitative data which may help to the understanding of the deposit properties. This article only focuses on the ions proportion in the sputtered vapor and more precisely on the proportion of the ionized material vapor flux located

in the post-discharge going towards the substrate (Hopwood 1998). The knowledge of this proportion allows a wide control over the final deposit.

For convenience and formalism, we note the proportion of ionized material flux Θ as the ratio between the flow of ionized target material Γi and the total flow (Γi + Γn) of heavy particles which are deposited at the surface of the substrate (Helmersson 2006), i.e $\Theta = \Gamma i/(\Gamma i + \Gamma n)$, with Γn the flow of neutrals.

As put forward by Poolcharuansin et al (2012), the knowledge of the ions proportion of the target material in gas phase is critical and some researchers deployed a wealth of ingenuity to find a way to know this ratio. In addition to the examples given by Poolcharuansin et al (Kouznetsov 1999; Macák 2000; Ehiasarian 2003; Nakamura 2007), Hubička et al (Hubička 2013; Kubart 2014; Stranak 2014; Lundin 2015) highlight the conception and the use of a gridless quartz microbalance. This specificity enables a good measurement of Θ in conditions where the sputtering target could be limited, like processes with very low rates of sputtering.

It should be noted that most studies use an improved quartz balance which allows to discriminate the heavy charges of the neutrals coming from the HiPIMS discharge. This is effectively a reliable and relatively uncomplicated solution.

In this article, the study focuses on a very easy way to use an unmodified quartz crystal microbalance (QCM) coupled to a grid energy analyzer (GEA) which is denoted as QCM-GEA. This simple method has already been used in the past (Fox 1994; Green 1997; Hayden 1998), but not in the case of platinum, gold, palladium and their mixed compositions ($Pt_{50}Au_{50}$ and Pt_5Pd_{95}) in HiPIMS. The reserves of these pure materials are in very limited quantities on Earth. Paradoxically, they are widely used in high-tech applications and catalytic applications (Yu 2012; Pakhare 2014). The study of these sputtering elements in HiPIMS process aims to comprehend the possibilities and the optimization of uses of these high potentials catalytic

materials. The knowledge of the Θ proportion for each of these noble materials depending on the discharge conditions is therefore a key data. The article purpose is then to highlight the use of the QCM-GEA as an efficient and an easy way to know this Θ proportion.

Experimental set up

As shown in Figure 1, the experimental setup consists of an cross-shaped UHV chamber in which the 6 flanges are connected to the pumping device (primary pump + Adixen ATH500M for a base pressure of 10^{-7} mbar), the gas mass flowmeters (Ar, Kr or Xe), a 2 inches magnetron with unbalanced magnetic configuration, an linear shift mechanisms on which the QCM-GEA apparatus is fixed. The 2 inches magnetron can be powered by either a HiPIMS generator (Hüttinger TPHS 4002) or by a DC power generator (Advanced Energy Pinnacle Plus). Each 2 inches target (Pt, Au, Pd, $Pt_{50}Au_{50}$ and Pt_5Pd_{95} used in this study) have a normalized thickness of 1524 µm and are bonded on a 3175 µm thick copper backing, thus enabling to make a comparative study with an iso magnetic topology for each target mounted on the magnetron device.

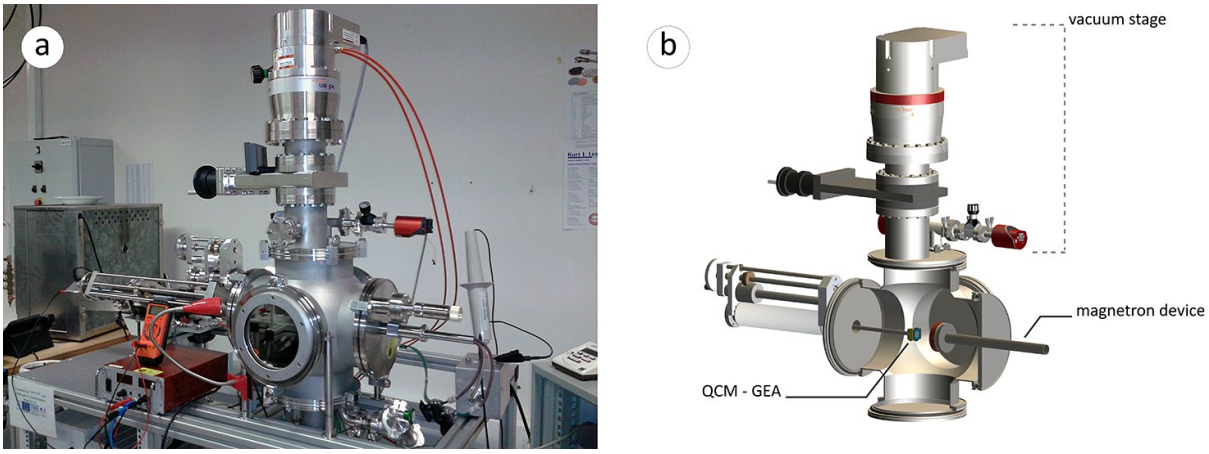

Figure 1: a) Picture of the experimental setup for the magnetron sputtering process. b) 3D View of the QCM-GEA system placed in front of the magnetron device.

Working processes are carried out with the injection of pure gas and without gas mixing. A UHV gate valve insures the pressure regulation in the vacuum chamber, fixed here to 10^{-2} mbar. The different gas flows are standardized on the argon flow for reaching the set pressure inside the vacuum chamber, either 4 sccm in Ar.

The discharge conditions are regulated for all experiments by using the HiPIMS voltage. The negative U_{HiPIMS} peak voltage ranges from an absolute value from 700 V to 2000 V, the pulse duration and frequency are respectively fixed to 100 µs and 50 Hz. The current and the voltage characteristics of the discharge are measured by the means of a high voltage probe (Tektronix P6015A) and a current probe (Stangenes CT0.5-0.1W) placed at the back of the magnetron system.

Figure 2 presents the QCM-GEA device based on a commercial Maxtek TM-400 QCM on which a homemade grid system is fixed. Figure 2 b) and c) exhibit the compactness of the QCM-GEA system. The QCM resolution can reach 0.01 $nm.s^{-1}$ for the deposition rate and 0.01 nm for the thickness. The GEA consists of a stack of two stainless steel wire mesh grids spaced by an 900 µm thick piece of milar (blue spacer) and electrically isolated (red spacer) from the body of the quartz microbalance. With a diameter of 12 mm, the GEA system opening is lightly higher than the 8 mm diameter of the quartz surface collection. The first grid, with 81 mesh/cm^2 and a wire diameter of 200 µm, is grounded to the experiment vessel and acts as a screen grid electrically separate from the plasma post-discharge and the second grid. This second grid, with 900 mesh/cm^2 and a wire diameter of 50 µm, allows to discriminate the ionized part of the metal vapor by the application of a positive potential (V_d), as a discriminating grid. Depending on the potential applied between the screen grid and the discriminating grid, the quartz microbalance behaves like an ion/neutral filter. When mounting the GEA system, a laser alignment of the

grids is not necessary since the screen grid and the discriminating grid don't have the same mesh dimension. The total transmission of the QCM-GEA system is then 18 %.

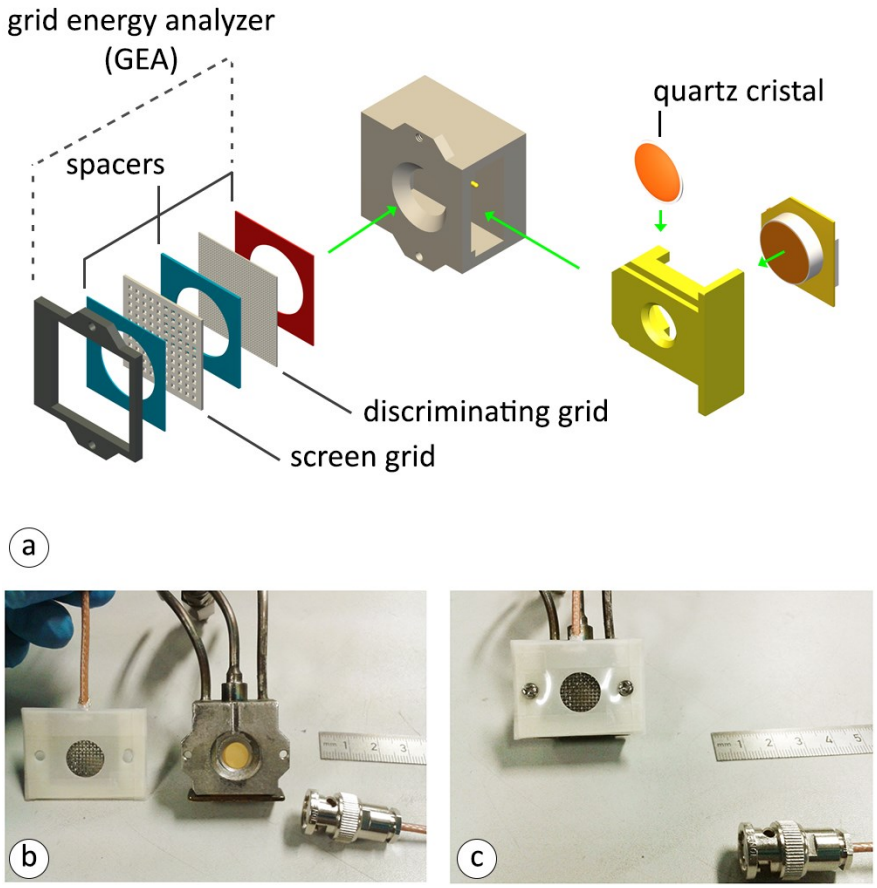

Figure 2 : a) Schematic of the quartz balance and the polarization system. b) and c) Assembling polarization system with quartz micro-balance to form the QCM-GEA.

The distance between the surface of the sputtering targets and the QCM-GEA is ranging from 40 mm to 75 mm during the experiments, which correspond to a classical range of distance for a such 2" sputtering magnetron device.

A homemade Labview software allows the control of the QCM-GEA system in order to collect the measurements performed by the QCM and to manage the potential applied on the discriminating grid. Depending of the experiments, a voltage ramp or a fixed voltage can be applied on the discriminating grid. The acquisition time is equal to 75 s when a voltage ramp is

applied on V_d (scan rate of 1 $V.s^{-1}$ between -15 V and + 60 V). For a fixed voltage V_d, the acquisition time of one measurement is set on 10 s. These durations are a compromise between the signal to noise ratio and the consumption of precious metals targets. For other inexpensive materials, time acquisitions should be increased in order to improve significantly the signal to noise ratio and therefore to obtain more accurate results.

First experiment measurements are done with the sputtering of the platinum target in argon gas by applying a negative HiPIMS voltage ranged between 1000 V and 1900 V and with a voltage step of 300 V. In this case the QCM-GEA position is successively placed at different distances from the target between 40 mm and 75 mm with 5 mm increments.

Second experiment gives the deposition rates obtained with the QCM-GEA set at 50 mm from the magnetron device in HiPIMS regime for Pt, Au, Pd, Pt_{50}-Au_{50} and Pt_5Pd_{95} targets and for different pure gases as Ar, Kr and Xe.

Results and discussion

This study begins with the sputtering of the platinum target in argon gas. Figure 3 reports the evolution of the Pt deposition rate as function of the voltage applied to the GEA discriminative grid (V_d) for the four negative HiPIMS voltages : (a) 1000 V, (b) 1300 V, (c) 1600 V and (d) 1900 V. The fifth and last figure e) corresponds to the Pt deposition rate performed in DCMS regime for an average power of 50 W. In order to do a comparative study, all the measurements of deposition rate are arbitrarily normalized to the deposition rate obtained with grounded discriminating grid (V_d = 0 V) in the sputtering HiPIMS regime, for a voltage of 1500 V which is equivalent to an average power of 50 W for our HiPIMS discharge conditions.

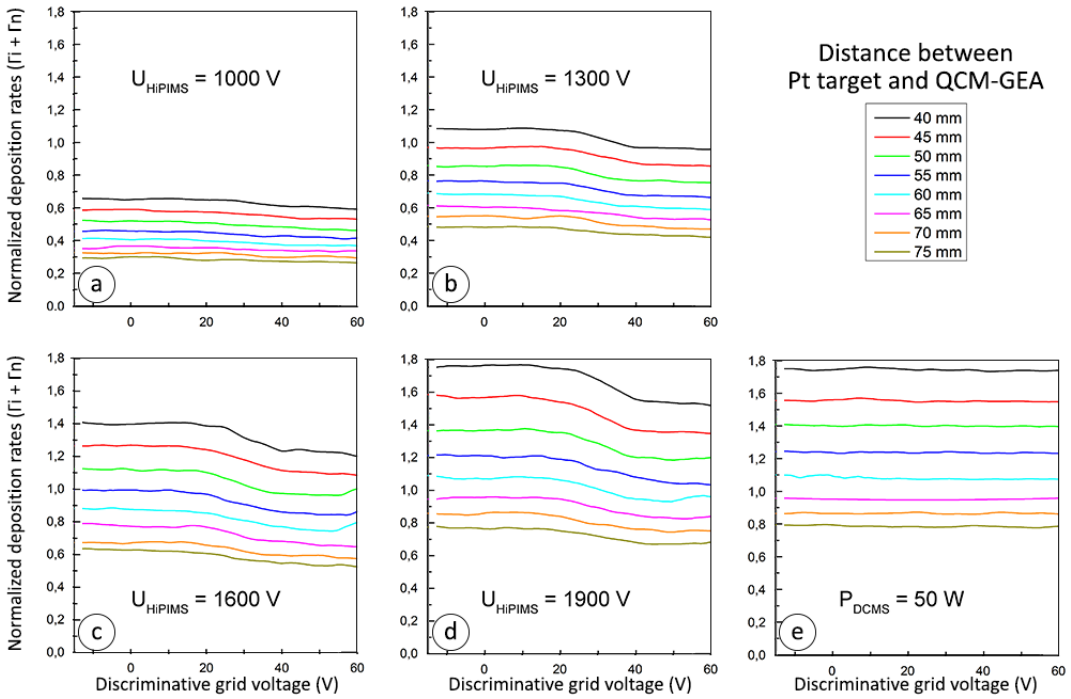

Figure 3: Deposition rate on the QCM-GEA as function of the discriminative voltage V_d , for various QCM-GEA/target distances and different U_{HiPIMS} : 1000 V, 1300 V, 1600 V, 1900 V. Deposition rates arbitrary normalized to the deposition rate of the U_{HiPIMS} equal to 1500 V and for a V_d null. Image at the down right corner shows results for a 50 W DCMS process.

Multiple results can be derived from this figure 3. Firstly, the increase of voltage applied on the discriminative grid up to a threshold value (approximately 20 V for each HiPIMS case) allows to separate the platinum ions of the total metallic vapor. This separation is characterized by a decrease in the deposition rate from 20 V whatever the distance between the QCM-GEA and the sputtering target is, and regardless the applied HiPIMS voltage. Between 0 V and 20 V, the atoms and the ions of platinum are collected on the quartz, while beyond 40 V, only the atoms come at the surface quartz. Since argon is a non-reactive gas, it is not necessary to worry about argon ions (also repealed) which can not intervene in the increase mass at the top surface of the QCM quartz. The phenomenon is observed for all HiPIMS cases. For example, for U_{HiPIMS} = 1000 V and a distance of 40 mm, the normalized deposition rate goes from 0.67 to 0.62 when discriminative grid voltage changes from 10 V to 40 V. According to the formalism previously

expressed, we obtain $(\Gamma i + \Gamma n)_{normalized} = 0.67$ et $\Gamma n_{normalized} = 0.62$. The ionization fraction Θ is about 0.08 which means that platinum ions compose 8% of the metal vapor assuming that the sticking coefficient of ions and neutral on the quartz are identical. This decrease of the deposition rate for a threshold voltage is observed for all graphs concerning HiPIMS regime. These results highlight the formal presence of Platinum ions in metal steam in HiPIMS regime. The increase of the HiPIMS discharge voltage does not seem to influence the proportion of ions in the metal vapour, and remains between 8% and 10%. Moreover, Θ does not vary with the distance between the QCM-GEA and the sputtering target. This result indicates that platinum ions do not undergo any inelastic collisions as volumic recombinations on the considered distance range. Since volumic recombinations are link to mean free paths, then the selected working pressure for our HiPIMS process seems to be in good agreement for the metal ions' use during the deposition.

Secondly, looking at the grid voltage V_d necessary to discriminate Γi, it would seem that the global energy of the metal ions remains stable between the two extreme positions of the QCM-GEA (40 mm and 75 mm). This suggests that metal ions also do not undergo of elastic collisions on their trajectories. We also note a division by a factor of about 2 of the deposition rate between the 40 mm and 75 mm positions. With the DCMS discharge at 50 W, the decrease of the deposition rate do not take place when increasing the discriminating grid voltage. Therefore, the metal vapor seems to be only composed of Pt atoms in DCMS. This comparison HiPIMS/DCMS highlights the different modes of production of species between the two regimes. However it is important to note that the deposition rate is higher in DCMS than in HiPIMS regime at the same average power of 50 W for the sputtering of the Pt target. This result corroborates those obtained with other elements in HiPIMS regime [Anders 2011; Čapek 2013; Lundin 2008; Alami 2006).

This study continues with the measurement of the deposition rates in HiPIMS regime on Pt, Au, Pd, $Pt_{50}Au_{50}$ and Pt_5Pd_{95} allied targets. The working pressure, the duration of the HiPIMS pulses and their frequency remains unchanged. Figure 4 gives an example of the measured target currents during a HiPIMS pulse voltage for each gas, here at U_{HiPIMS} = 1500 V. The position of the QCM-GEA is set at 50 mm from the magnetron. The deposition rates are also normalized to those obtained by HiPIMS with Ar gas and reporting targets (Pt, Au, Pd, $Pt_{50}Au_{50}$ or Pt_5Pd_{95}), for U_{HiPIMS} = 1500 V. As above, Θ is determined by the evolution of the normalized deposition rates depending of the positive bias V_d.

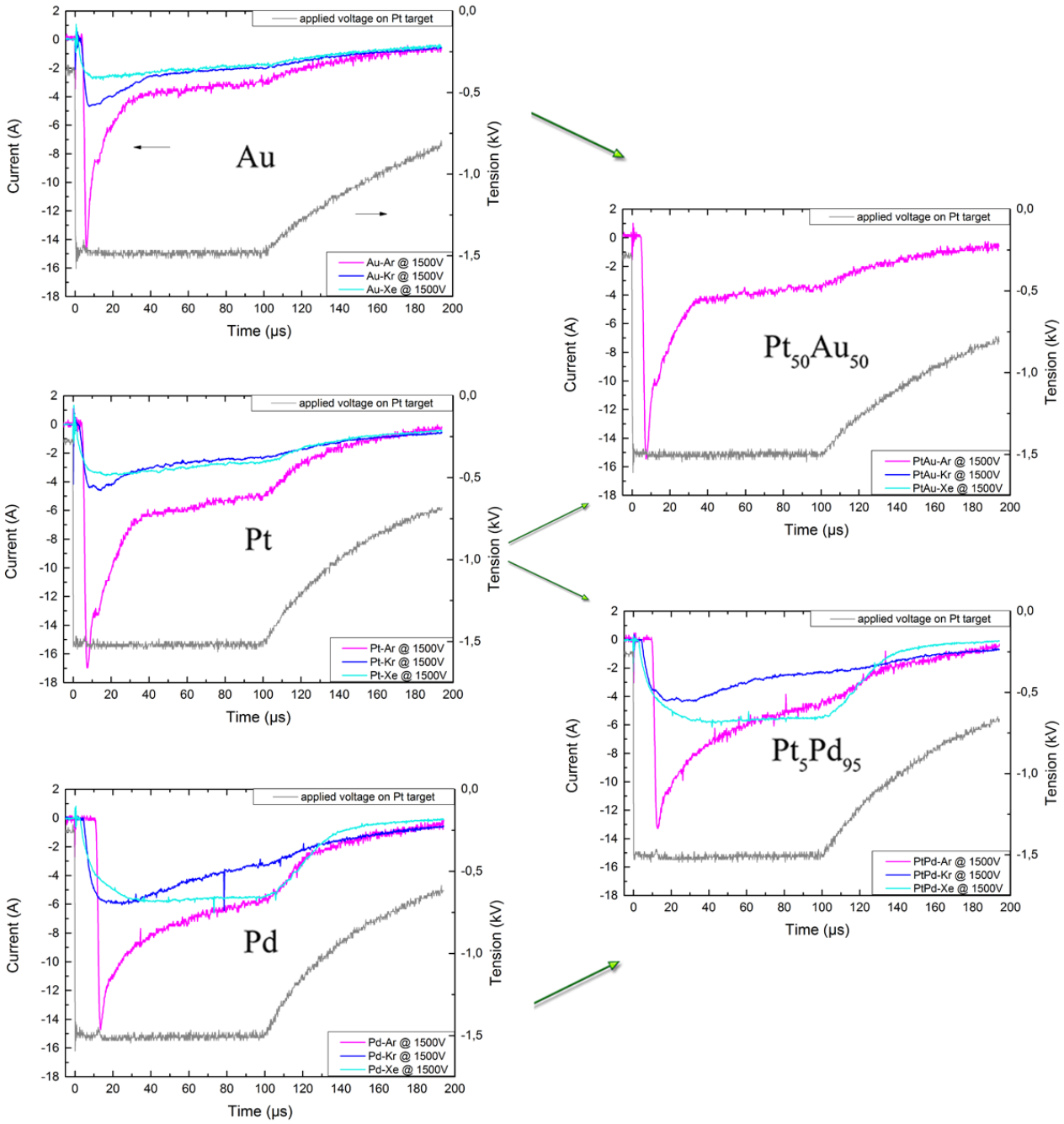

Figure 4: Target currents at -1500 U_{HiPIMS}, pulse duration 100 µs, frequency 50 Hz, for different targets and gases : respectively Au, Pt, Pd, $Pt_{50}Au_{50}$, Pt_5Pd_{95} and Ar, Kr, Xe.

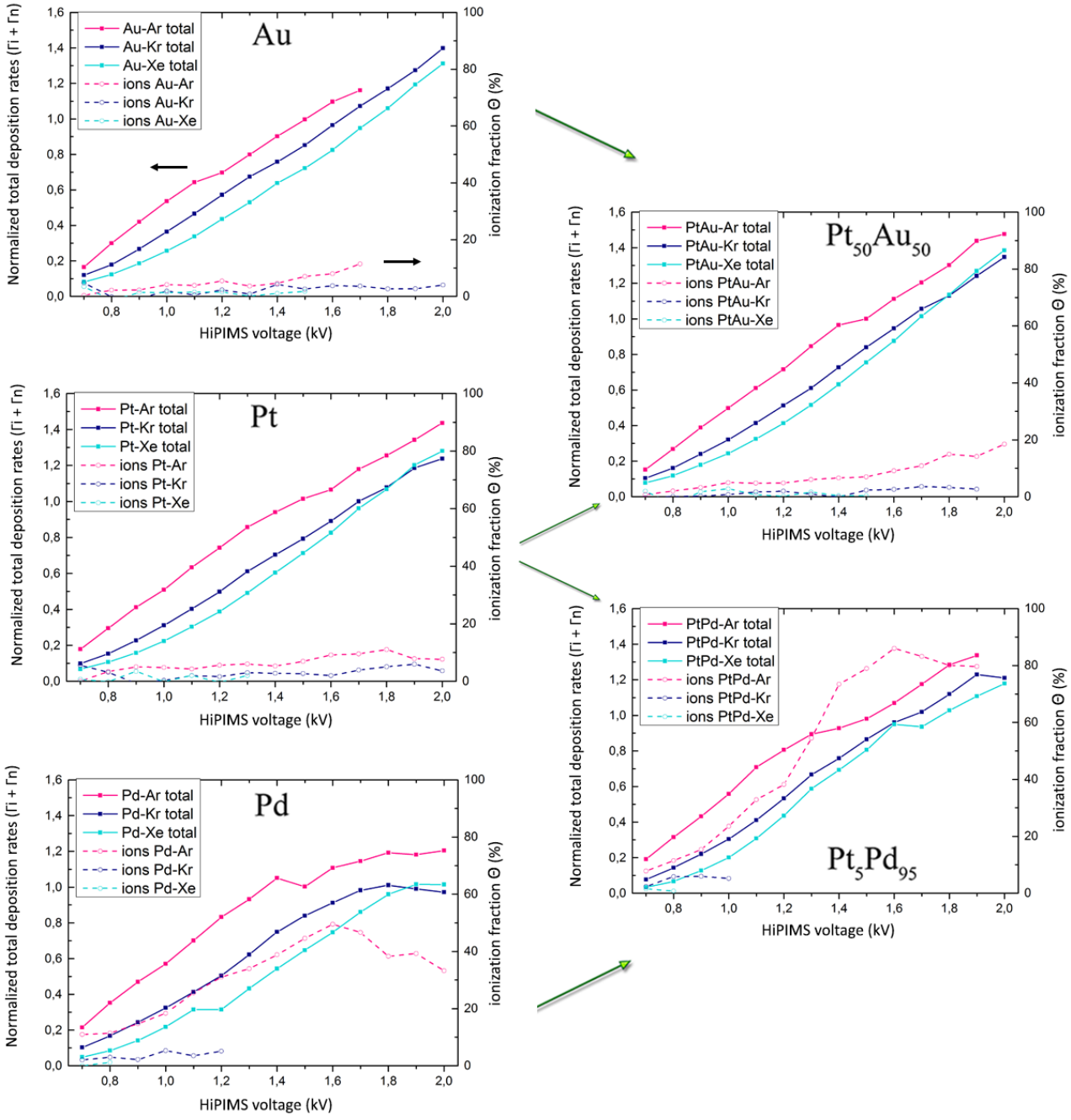

Figure 5: QCM-GEA normalized deposition rate (full lines) and ions/neutrals ratio Θ (dashed lines) as a function of U_{HiPIMS} , for different targets and gases : respectively Au, Pt, Pd, $Pt_{50}Au_{50}$, Pt_5Pd_{95} and Ar, Kr, Xe.

Figure 5 reflects all the measurements done in Ar, Kr, and Xe gases. Each graph is attributed to a specific target material : Pt, Au, Pd, $Pt_{50}Au_{50}$ or Pt_5Pd_{95}. Normalized deposition rates are

represented in full line while the different Θ (noted as a percentage (%) on the secondary vertical value axis) are represented by dashed lines. In a first time and by a correlation with the pulse discharge currents from Figure 4, three major observations on normalized deposition rates can be drawn:

- the deposition rate quasi-linearly increases with the HiPIMS voltage for all cases except for the Pd target (and Pt_5Pd_{95} to a lesser extent) where a saturation is observed from 1600 V with Ar and Kr gas (and from 1800 V in Xe gas). A relationship of proportionality between deposition rates and target current exists for each material in function of a distinct plasmogen gas, as it was already report (Sarakinos 2010).

- the nature of the gas plays an important role on the deposition rate in HiPIMS regime for each metal targets. This result is globally visible if we compare the different pulse discharge currents collected on a considered target of the figure 4 with the respective deposition rate of the Figure 5. In some cases, the deposition rate values found for distinct gases are different even if the pulse discharge currents collected on the considered target are similar, therefore a similar mean power.

- Argon (pink) allows to get the highest deposition rate for a fixed HiPIMS voltage. Kr (dark blue) comes in second position, followed by Xe (cyan). This result is reversed in Kr and Xe for a HiPIMS voltage higher than 1800 V in the case of the Pt, $Pt_{50}Au_{50}$ and Pd sputtering target.

In a second time, all the ion proportions could not be measured. In some cases, increasing the voltage Vd on the GEA causes the appearance of a secondary plasma near the screen grid, affecting the initial Θ parameter in the metal vapor. This phenomenon mainly occurs for Xe and to a lesser extent for Kr for high HiPIMS voltage values. Indeed, increasing the voltage V_d to positive values allows to attract and to give energy to few secondary electrons (initially

repelled by the first grid) which can generate this visible secondary plasma. This difficulty could have been overcome by the simple addition of a so-called *repeller* grid sandwiched between the screen grid and the discriminative grid. Once done, it would have been enough to repel the electrons coming from the magnetron plasma. The counterpart of this alternative is the decrease of the GEA transparency and so the decrease of particles flux coming onto the quartz surface. It was not done due to the sputtering target prices. Therefore, this solution reduces the resolution of the detection of the deposition rate and therefore mechanically, that of Θ. The alternative is to leave on systems more developed as those written in the introduction (eg. gridless quartz microbalance of Hubička Z. et al [23-26]). Figure 5 only shows the valid measures on the ion proportions.

With the Pt target, a maximum ion proportion of about 10% is found in the metal vapor in Ar gas. The proportion of ionized material Θ appears to increase slightly with the HiPIMS voltage, then it starts to decrease from 1800 V. The use of the Kr gas makes Θ lower than 5% all over the HiPIMS voltage range. With Xe gas the proportion of ionized material is much lower than with Kr and tends to 0 %. The Au target gives similar results with nevertheless a lowest Θ in Ar gas (between 5 and 10%), compared to the Pt target. The use of the Pd target gives a high ratio of metal ions in Ar gas with a Θ reaching more than 50 % at 1600 V. This proportion then declines to 32 % for a 2000 V HiPIMS voltage. It appears that increasing the HiPIMS beyond 1600 V voltage does not promote the increase of the proportion of Pd ions in the post discharge metal vapor. A return of these metal ions in direction of the negatively polarized target is a track considered to explain this fall in the ratio. The $Pt_{50}Au_{50}$ target reflects similar Θ to those found in the case of pure Pt and Au targets. Nevertheless, the ratio is slightly higher in the case of the mixed target in Ar gas, with a maximum value of about 19 %. In contrast, the Pt_5Pd_{95} target gives a proportion of ions with the use of Ar gas well above those found with the pure Pd target. In this case Θ is close to 90 %. The 5 % atomic Pt doping seems to play a key role in the increase

of the value of the ratio Θ for a fixed HiPIMS voltage. This result seems to be confirmed for a few measurements done with Kr gas (without the ignition of the secondary plasma near the QCM-GEA). As for the pure Pd target, the ratio of ions decreases from 1600 V in Ar gas.

It should be noted finally that experimentally the use of Kr and Xe gas do not favor the production of metal ions nor, in most cases, an increase of the deposition rates in the HiPIMS post-discharge. However, they present respectively higher masses (83.80 amu and 131.29 amu) than Ar (39.948 amu) and lower first ionization threshold energy (13.9996 eV and 12.1298 eV) than Ar (15.7596 eV). Future tests should be done in Ne and He gases to see if the trends are reversing and to point out the fine physical mechanisms involved in the obtained Θ ratios.

Conclusion

The use of a QCM-GEA allowed us to study the metal vapor in HiPIMS regime and to confirm the presence of charged metal species in most of studied cases. This compact and efficient system of measurement allows to access to the deposition rates but also to key physical properties as the ionized proportion of the sputtered vapor in HiPIMS regime. The maximum proportions Θ found in Ar gas are 10 % for Pt, 12 % for Au, 50 % for Pd, 19 % for $Pt_{50}Au_{50}$ and 88 % for Pt_5Pd_{95} target. By using the QCM-GEA, we highlight that it's not necessary to use the Kr or Xe gas instead of Ar gas since both of them drastically reduces these proportions. The increase of the ion proportion when 5% Pt doping is added in the Pd target indicates that such Pt doping plays a key role in the ionization mechanisms of the metallic vapor. Other measurements should be done in Ne or He gases in order to explore possibilities to increase the Θ proportion.

Acknowledgements

CEA is acknowledged for a grant. The European commission is acknowledged for funding part of this work through the European Regional Development Fund (ERDF).

References

Ait Aissa, K., Achour, A., Camus, J., Le Brizoual, L., Jouan, P.Y., and Djouadi, M.A. 2014 Comparison of the structural properties and residual stress of AlN films deposited by dc magnetron sputtering and high power impulse magnetron sputtering at different working pressures *Thin Solid Films* **550** 264–7

Alami, J., Persson, P.O.A., Music, D., Gudmundsson, J.T., Bohlmark, J., and Helmersson, U. 2005 Ion-assisted physical vapor deposition for enhanced film properties on nonflat surfaces *Journal of Vacuum Science & Technology A: Vacuum, Surfaces, and Films* **23** 278

Alami, J., Sarakinos, K., Mark, G., and Wuttig, M. 2006 On the deposition rate in a high power pulsed magnetron sputtering discharge. *Applied Physics Letters* **89,** 154104

Anders, A., 2008 Self-sputtering runaway in high power impulse magnetron sputtering: The role of secondary electrons and multiply charged metal ions *Applied Physics Letters* **92** 201501

Anders, A. 2011 Discharge physics of high power impulse magnetron sputtering *Surface and Coatings Technology* **205, Supplement 2** S1–9

Baghriche, O., Ehiasarian, A.P., Kusiak-Nejman, E., Pulgarin, C., Sanjines, R., Morawski, A.W., and Kiwi, J. 2012 High power impulse magnetron sputtering (HIPIMS) and traditional pulsed sputtering (DCMSP) Ag-surfaces leading to E. coli inactivation *Journal of Photochemistry and Photobiology A: Chemistry* **227** 11–7

Čapek, J., Hála, M., Zabeida, O., Klemberg-Sapieha, J. E., and Martinu, L. 2013 Deposition rate enhancement in HiPIMS without compromising the ionized fraction of the deposition flux. *J. Phys. D: Appl. Phys.* **46,** 205205

Cuynet, S., Caillard, A., Lecas, T., Bigarré, J., Buvat, P., and Brault, P., 2014 Deposition of Pt inside fuel cell electrodes using high power impulse magnetron sputtering *J. Phys. D: Appl. Phys.* **47** 272001

Ehiasarian, A.P., Münz, W.D., Hultman, L., Helmersson, U., and Petrov, I. 2003 High power pulsed magnetron sputtered CrNx films *Surface and Coatings Technology* **163–164** 267–72

Fox, Gr., and Krupanidhi, S b. 1994 Dependence of perovskite/pyrochlore phase formation on oxygen stoichiometry in PLT thin films *Journal of Materials Research* **9** 699–711

Green, K.M., Hayden, D.B., Juliano, D.R., and Ruzic, D.N. 1997 Determination of flux ionization fraction using a quartz crystal microbalance and a gridded energy analyzer in an ionized magnetron sputtering system *Review of Scientific Instruments* **68** 4555–60

Hayden, D.B., Juliano, D.R., Green, K.M., Ruzic, D.N., Weiss, C.A., Ashtiani, K.A., and Licata, T.J. 1998 Characterization of magnetron-sputtered partially ionized aluminum deposition *Journal of Vacuum Science & Technology A* **16** 624–7

Helmersson, U., Lattemann, M., Bohlmark, J., Ehiasarian, A.P., and Gudmundsson, J.T. 2006 Ionized physical vapor deposition (IPVD): A review of technology and applications *Thin Solid Films* **513** 1–24

Hopwood, J. 1998 Ionized physical vapor deposition of integrated circuit interconnects *Physics of Plasmas* **5** 1624

Hovsepian, P. E., Ehiasarian, A. P., and Petrov, I., 2014 Structure evolution and properties of TiAlCN/VCN coatings deposited by reactive HIPIMS *Surface and Coatings Technology* **257** 38–47

Hubička, Z., Kment, Š., Olejníček, J., Čada, M., Kubart, T., Brunclíková, M., Kšírová, P., Adámek, P. and Remeš, Z. 2013 Deposition of hematite Fe2O3 thin film by DC pulsed magnetron and DC pulsed hollow cathode sputtering system *Thin Solid Films* **549** 184–91

Konstantinidis, S., Dauchot, J.P., and Hecq, M. 2006 Titanium oxide thin films deposited by high-power impulse magnetron sputtering *Thin Solid Films* **515** 1182–6

Kouznetsov, V., Macák, K., Schneider, J. M., Helmersson, U., and Petrov, I. 1999 A novel pulsed magnetron sputter technique utilizing very high target power densities *Surface and Coatings Technology* **122** 290–3

Kubart, T., Čada, M., Lundin, D., and Hubička, Z. 2014 Investigation of ionized metal flux fraction in HiPIMS discharges with Ti and Ni targets *Surface and Coatings Technology* **238** 152–7

Lin, J., Sproul, W.D., Wei, R., and Chistyakov, R. 2014 Diamond like carbon films deposited by HiPIMS using oscillatory voltage pulses *Surface and Coatings Technology* **258** 1212–22

Lundin, D., Larsson, P., Wallin, E., Lattemann, M., Brenning, N., and Helmersson, U. 2008 Cross-field ion transport during high power impulse magnetron sputtering. *Plasma Sources Sci. Technol.* **17,** 35021

Lundin, D., Čada, M., and Hubička, Z. 2015 Ionization of sputtered Ti, Al, and C coupled with plasma characterization in HiPIMS *Plasma Sources Sci. Technol.* **24** 035018

Macák, K., Kouznetsov, V., Schneider, J., Helmersson, U., and Petrov, I. 2000 Ionized sputter deposition using an extremely high plasma density pulsed magnetron discharge *Journal of Vacuum Science & Technology A* **18** 1533–7

Nakamura, K., Wakayama, A., and Yukimura, K. 2007 Effects of reactive gas addition on ionization of metal atoms in droplet-free metal ion sources *Surface and Coatings Technology* **201** 6655–9

Nakao, S., Yukimura, K., Nakano, S., and Ogiso, H. 2013 DLC Coating by HiPIMS: The Influence of Substrate Bias Voltage *IEEE Transactions on Plasma Science* **41** 1819–29

Pakhare, D., and Spivey, J. 2014 A review of dry (CO2) reforming of methane over noble metal catalysts *Chem. Soc. Rev.* **43** 7813–37

Partridge, J.G., Mayes, E.L.H., McDougall, N.L., Bilek, M.M.M., and McCulloch, D.G. 2013 Characterization and device applications of ZnO films deposited by high power impulse magnetron sputtering (HiPIMS) *J. Phys. D: Appl. Phys.* **46** 165105

Poolcharuansin, P., Bowes, M., Petty, T.J., and Bradley, J.W. 2012 Ionized metal flux fraction measurements in HiPIMS discharges *J. Phys. D: Appl. Phys.* **45** 322001

Ratova, M., West, G.T., and Kelly, P.J., 2014 Optimisation of HiPIMS photocatalytic titania coatings for low temperature deposition *Surface and Coatings Technology* **250** 7–13

Samuelsson, M., Lundin, D., Jensen, J., Raadu, M.A., Gudmundsson, J.T., and Helmersson, U. 2010 On the film density using high power impulse magnetron sputtering *Surface and Coatings Technology* **205** 591–6

Sarakinos, K., Alami, J., Konstantinidis, S. 2010 High power pulsed magnetron sputtering: A review on scientific and engineering state of the art. *Surface and Coatings Technology* **204,** 1661-1684

Stranak, V., Hubicka, Z., Cada, M., Drache, S., Tichy, M., and Hippler, R. 2014 Investigation of ionized metal flux in enhanced high power impulse magnetron sputtering discharges *Journal of Applied Physics* **115** 153301

Velicu, I.L., Neagu, M., Chiriac, H., Tiron, V., and Dobromir, M. 2012 Structural and Magnetic Properties of FeCuNbSiB Thin Films Deposited by HiPIMS *IEEE Transactions on Magnetics* **48** 1336–9

Wang, Z., Zhang, D., Ke, P., Liu, X., and Wang, A., 2015 Influence of Substrate Negative Bias on Structure and Properties of TiN Coatings Prepared by Hybrid HIPIMS Method *Journal of Materials Science & Technology* **31** 37–42

Yu, W., Porosoff, M.D., and Chen, J.G. 2012 Review of Pt-Based Bimetallic Catalysis: From Model Surfaces to Supported Catalysts *Chem. Rev.* **112** 5780–817